Journal of Electrical Engineering & Technology Vol. 6, No. 6, pp. 731~741, 2011 **731**
http://dx.doi.org/10.5370/JEET.2011.6.6.731

Type-2 Fuzzy Logic Optimum PV/inverter Sizing Ratio for Grid-connected PV Systems: Application to Selected Algerian Locations

S. Makhloufi† and R. Abdessemed*

Abstract – Conventional methodologies (empirical, analytical, numerical, hybrid, etc.) for sizing photovoltaic (PV) systems cannot be used when the relevant meteorological data are not available. To overcome this situation, modern methods based on artificial intelligence techniques have been developed for sizing the PV systems. In the present study, the optimum PV/inverter sizing ratio for grid-connected PV systems with orientation due south and inclination angles of 45° and 60° in selected Algerian locations was determined in terms of total system output using type-2 fuzzy logic. Because measured data for the locations chosen were not available, a year of synthetic hourly meteorological data for each location generated by the PVSYST software was used in the simulation.

Keywords: Grid-connected, Maximum power point tracker (MPPT), Photovoltaic, Sizing ratio, Tilted angle, Type-2 Fuzzy logic

1. Introduction

The optimum output of a grid-connected photovoltaic (PV) system depends on the relative size of photovoltaic array and inverter [1-3, 5, 11, 13]. The sizing ratio (R) is defined as the ratio of the rated inverter input power to the PV array capacity at standard test conditions (STCs) given as follows:

$$R = \frac{P_{inv,rated}}{P_{pv,rated}} \quad (1)$$

where $P_{pv,rated}$ and $P_{inv,rated}$ represent rated PV capacity and rated inverter input power, respectively.

Optimal PV/inverter sizing depends on local climate, PV surface orientation and inclination, inverter performance, and PV/inverter cost ratio [13–15]. Under low insolation, a PV array generates power for only a part of its rated capacity. The inverter thus operates under partial load conditions with lower system efficiency. PV efficiency is also affected adversely. When an inverter's rated capacity is much lower than the PV rated capacity, the inverter operates under overload conditions. Under overloading condition, excess PV output greater over the inverter rated capacity is lost. An oversized or undersized inverter thus increases PV energy cost [2, 10].

Conventional methodologies (empirical, analytical, numerical, hybrid, etc.) for sizing PV systems are generally used when the required weather data (irradiance, temperature, humidity, clearness index, wind speed, etc.) and the information concerning the location of PV system are available. These methods present a good solution for sizing PV systems under the above conditions. However, such techniques cannot be used for sizing PV systems where the required data are not available. Moreover, the majority of the above methods need long-term meteorological data, such as total solar irradiance, air temperature, and wind speed, for their operations.. To overcome this situation, newer methods have been developed for sizing the parameters for PV systems based on artificial intelligence techniques [17].

Type-1 fuzzy logic has been used in many works for sizing PV systems [17]. However, using type-1 fuzzy logic for this aim requires the experience and knowledge of human experts to decide both the membership functions and the fuzzy rules. Because the membership grade of the type-1 fuzzy system is a crisp number in (0,1), it is unable to directly handle rule uncertainties. In addition, words used in the fuzzy rules can often mean different things to different people. This results in rule uncertainty with the available information.

To tackle this problem, Zadeh [27] proposed the concept of type-2 fuzzy system, which is an extension of type-1 fuzzy system. Type-2 fuzzy system is also characterized by IF-THEN rules; however, its membership functions are type-2 fuzzy sets. The structures of type-1 and type-2 fuzzy systems are shown in Fig. 1. The structure of a type-2 fuzzy system is very similar to the structure of a type-1 fuzzy system, with differences only in the output processing. The output processor includes a type reducer and a defuzzifier to generate a type-1 fuzzy system output from the type reducer or a crisp number from the defuzzifier. Thus, the type reduction captures more information about rule uncertainties

† Corresponding Author: LEB Research Laboratory, University of Batna, Algeria (Makhlofi_s@hotmail.com)
* LEB Research Laboratory, University of Batna, Algeria (rachid.abdessemed@gmail.com).
Received: July 31, 2010; Accepted: June 15, 2011

than does the defuzzified value (a crisp number). A type-2 fuzzy system is characterized by a fuzzy membership function, that is, the membership grade for each element is a fuzzy set in (0,1). This is unlike the type-1 fuzzy system, in which the membership grade is a crisp number in (0,1). Thus, a type-2 fuzzy system is very useful in circumstances in which the membership grades are difficult to exactly determine [27], [28].

In the present study, type-2 fuzzy logic is used to determine optimum PV/inverter sizing ratios for grid-connected PV systems with orientation due south and inclination angles of 45° and 60° in selected Algerian locations in terms of total system output. In short, the optimum PV/inverter sizing ratios are determined to maximize the total power generated by the PV system. Because measured data in the locations chosen were not available, for each location, a year of synthetic hourly meteorological data was used in the simulation. Monthly meteorological data available on the NASA Web site [30] were used for the generation of hourly synthetic meteorological data (horizontal global irradiance and ambient temperature) using the PVSYST software [23].

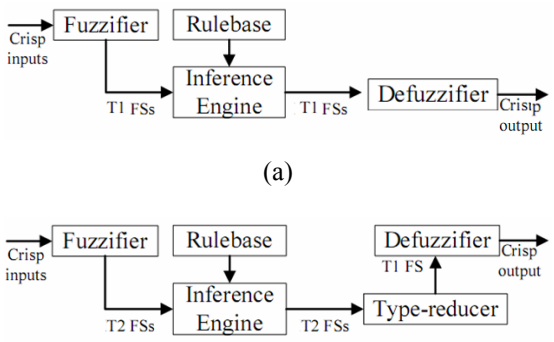

Fig. 1. The structure of the fuzzy systems: (a) Type-1 fuzzy systems; (b) Type-2 fuzzy systems

2. Mathematical modeling

2.1 Photovoltaic array output modeling

The "four-parameter" equivalent circuit model that considers a PV cell as an "ideal" irradiance-dependent current source in parallel with a diode was used to model the PV module [4]. The four parameters are module photocurrent at reference conditions ($I_{L,ref}$), diode reverse saturation current at reference conditions ($I_{o,ref}$), empirical diode PV curve fitting factor (d_1), and module series resistance (R_s) [25]. The total current (I) is calculated as follows [26]:

$$I = I_L - I_0\left[\exp\left(\frac{q}{d_1 k T_c}\left(V + IR_s\right)\right) - 1\right] \tag{2}$$

The values of parameters d_1 and R_s are fixed for a given PV cell. The photocurrent (I_L) is linearly proportional to the incident irradiance:

$$I_L = I_{L,ref}\frac{I_T}{I_{T,ref}} \tag{3}$$

where $I_{L,ref}$ is the photocurrent at the reference conditions and I_T and $I_{T,ref}$ represent incident irradiance at any time and reference insolation, respectively, where the reference insolation is equal to 1000 W/m^2.

The reverse saturation current (I_o) is expressed in terms of material characteristics and PV module temperature (T_c):

$$I_o = I_{o,ref}\left(\frac{T_c}{T_{c,ref}}\right)^3 \exp\left[\frac{q\varepsilon}{dk}\left(\frac{1}{T_{c,ref}} - \frac{1}{T_c}\right)\right] \tag{4}$$

where d is equal to d_1 / n_s; n_s is the number of cells in the module connected in series; ε is the semiconductor band-gap energy; and $I_{o,ref}$ and $T_{c,ref}$ are reverse saturation current and module temperature, respectively, at reference conditions.

The parameters $I_{L,ref}$, $I_{o,ref}$, and d_1 can be derived from the general I–V expressions [i.e., Eq. (2)] at the reference conditions ($I_{T,ref}$ and $T_{c,ref}$). By substituting the current and voltage at the open circuit where current (I) is zero and voltage (V) is $V_{oc,ref}$ [Eq. (5)], the short circuit where voltage (V) is zero and current (I) is $I_{sc,ref}$ [Eq. (6)], and the maximum power point (MPP) conditions where current (I) is $I_{mp,ref}$ and voltage (V) is $V_{mp,ref}$ [Eq. (7)], the following equations are obtained:

$$0 = I_{L,ref} - I_{o,ref}\left[\exp\left(\frac{qV_{oc,ref}}{d_1 k T_{c,ref}}\right) - 1\right] \tag{5}$$

$$I_{sc,ref} = I_{L,ref} - I_{o,ref}\left[\exp\left(\frac{qI_{sc,ref}R_S}{d_1 k T_{c,ref}}\right) - 1\right] \tag{6}$$

$$I_{mp,ref} = I_{L,ref} - I_{o,ref}\left[\exp\left(\frac{q}{d_1 k T_{c,ref}}\left(V_{mp,ref} + I_{mp,ref}R_S\right)\right) - 1\right] \tag{7}$$

The magnitude of the reverse saturation current (I_o) is very small, generally in the order of 10^{-5} or 10^{-6}. The term "-1" in Eqs. (5), (6), and (7) can be neglected. For the short-circuit condition, the exponential term in Eq. (6) is very small and can therefore be neglected. These considerations lead to the following three expressions:

$$I_{o,ref} = \frac{I_{sc,ref}}{\exp\left(\frac{qV_{oc,ref}}{d_1 k T_{C,ref}}\right)} \tag{8}$$

$$I_{L,ref} \approx I_{sc,ref} \tag{9}$$

$$d_1 = \frac{q\left(V_{mp,ref} - V_{oc,ref} + I_{mp,ref} R_S\right)}{kT_{C,ref} \ln\left(1 - \frac{I_{mp,ref}}{I_{sc,ref}}\right)} \tag{10}$$

The parameter R_s is obtained from the temperature coefficients of the open-circuit voltage and short-circuit current ($\mu_{V,oc}$ and $\mu_{I,sc}$).

The values of these temperature coefficients are available from a PV module catalogue. The analytical derivative of voltage with respect to temperature at the reference open-circuit condition is matched to the open-circuit temperature coefficient of the voltage [25]:

$$\frac{\partial V_{oc}}{\partial T} = \mu_{V,oc} = \frac{d_1 k}{q}\left[\ln\left(\frac{I_{sc,ref}}{I_{o,ref}}\right) + \frac{T_C \mu_{I,sc}}{I_{sc,ref}} - \left(3 + \frac{q\varepsilon}{d_1 k T_{C,ref}}\right)\right] \tag{11}$$

The equivalent circuit characteristic parameters were calculated using MATLAB "solve" function to solve these four equations [i.e., Eqs. (8)–(11)].

According to the values shown in Table 1,

$$I_{o,ref} = 2.86 \times 10^{-6}\, A$$
$$R_s = 0.2421\ \Omega$$
$$d_1 = 120$$

The PV module characteristic parameters used in the study are shown in Table 1.

Table 1. PV module and array characteristic parameters

Parameter	value
Module short-circuit current at reference conditions	3.45 A
Module open-circuit voltage at reference conditions	43.5 V
Temperature at reference conditions	298 K
Irradiance at reference conditions	1000 W/m^2
Maximum power point voltage at reference conditions	35.0 V
Maximum power point current at reference conditions	3.15 A
Temperature coefficient of short-circuit current	4.0· 10^{-4}
Temperature coefficient of open-circuit voltage	-3.4· 10^{-3}
Semiconductor band gap	1.12 eV
Number of cells in the module connected in series	72
Number of modules in series in each subarray	17
Number of subarrays in parallel	7

2.2 Inverter output modeling

In reality, inverter efficiency is not constant; rather, it is a function of input power. To predict inverter output, the following equation is used [4]:

$$P_{inv,n} = k_0 + k_1 P_{pv,n} + k_2 P_{pv,n}^2 \tag{12}$$

where $P_{pv,n} = \frac{P_{pv}}{P_{inv,rated}}$ and $P_{inv,n} = \frac{P_{inv}}{P_{inv,rated}}$.

Here, $P_{pv,n}$ and $P_{inv,n}$ are the normalized inverter input and output power, respectively; $P_{inv,rated}$ is the rated inverter input capacity; and k_0, k_1, and k_2 are correlation coefficients. For the present study, the coefficients k_0, k_1, and k_2 were taken as -0.015, 0.98, and -0.09, respectively [4]. The inverter efficiency in relation to the input power is given in Fig. 2.

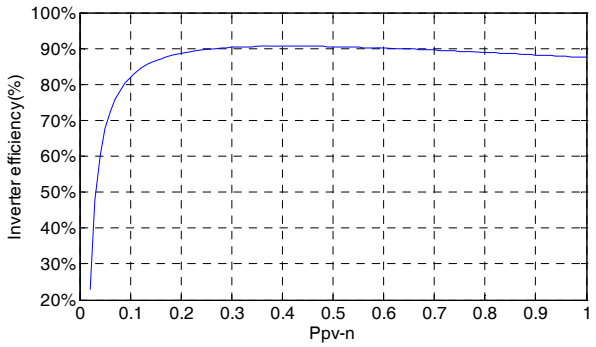

Fig. 2. Inverter efficiency

3. Meteorological data computation

Monthly meteorological data available on the NASA Web site [30] were used for the generation of hourly synthetic meteorological data (horizontal global irradiance and ambient temperature) with the aid of PVSYST software [23].

3.1 Horizontal global irradiance generation (I_G)

For global irradiance, PVSYST uses well-established random algorithms that produce hourly distributions of statistical properties very close to real data [20, 21].

The algorithm first uses PVSYST to construct a random sequence of daily values with the aid of a library of Markov transition matrices (probability matrices) constructed from real meteorological hourly data of several stations all over the world. It then applies a time-dependent, autoregressive, Gaussian model to generate the hourly sequences for each day.

3.2 Ambient temperature generation (T_a)

For temperature, a general model does not exist. PVSYST uses procedures adjusted only on Swiss meteorological data, for which generalization to any world climate is not proven.

In fact, the ambient temperature daily sequence shows only weak correlations to global irradiance. Because the temperature should be continuous, PVSYST constructs this sequence using essentially randomly daily slopes, with constraints on the monthly average.

However, a daily profile can be much more related to the global irradiance. During the day, temperature behaves similarly to a sinusoid, with amplitude related to the global daily irradiance, and a phase shift of 2–3 h. The corresponding correlation parameters (for amplitude and phase shift) are quantified from several Swiss region typologies, which can be generalized to analogous typologies for other places in the world.

The dependence of PV system behavior is not very temperature-sensitive (approximately 0.4%/°C). Provided that the monthly average is correct, the global results of the PV production will not strongly depend on the temperature daily sequence.

3.3 Module temperature

To determine module temperature, a simple equation was developed in [4] using module ambient temperatures and incident insolation data. The correlation equation is given by the following:

$$T_C = T_A + 0.031 I_T \tag{13}$$

3.4 Predicting hourly solar irradiance on inclined surface

In many sites, at best, only global irradiances on horizontal planes are available. Because most systems using solar energy are tilted, these data are clearly insufficient. A number of models to estimate global irradiance on an inclined surface from the irradiance on a horizontal surface are available; however, these models require information at the same time on the global and the direct or diffuse irradiance on a horizontal surface. In [9], two models requiring only the global irradiance on horizontal planes as input parameter were developed. The present work uses the model given in Eq. (14), which yields better results:

$$I_{T,\beta} = I_G \left[0.1 + \frac{\rho}{2} + \left(0.1 - \frac{1}{2}\rho \right) \cos\beta + 0.8 \left(\cos\theta / \cos\theta_z \right) \right] \tag{14}$$

where

$I_{T,\beta}$: total irradiance received on a tilted surface,
I_G : the horizontal global irradiance,
θ_z : the zenith angle calculated by [22]:

$$\cos\theta_z = \sin\delta \sin\phi + \cos\delta \cos\phi \cos\omega \tag{15}$$

δ : the declination of day D calculated by [6]:

$$\delta(D) = 0.4093 \sin\left(2\pi \frac{D - 81}{365} \right) \tag{16}$$

ρ : the albedo (in this work, a constant value for the albedo is equal to 0.2),
ϕ : the geographic latitude,
ω : the hour angle, and
θ : the angle of incidence for an arbitrarily inclined surface oriented toward the equator calculated by the following:

$$\cos\theta = \sin\delta \sin(\phi - \beta) + \cos\delta \cos(\phi - \beta) \cos\omega . \tag{17}$$

In the present study, a discrete form of the hour angle ω is chosen. The action of the sun moving in the sky can be replaced by irradiance in short time intervals of "many immovable suns" [6] whose positions correspond to the average position of the existing sun at the same time. If solar time is divided into sufficiently short time intervals, such a description will correspond to the description of an immovable sun. Temporary sun positions are considered uniformly distributed in solar time across time intervals; hence, they will be uniform with respect to hour angle. Time Δt can be obtained from the division of 24 h into N equal parts:

$$\Delta t = \frac{24}{N} \tag{18}$$

The variable n, which is symmetrical in relation to 12.00, is introduced according to the following formula:

$$\tau = n\Delta t + 12 \tag{19}$$

where τ is the solar time.

The equation for the determination of the hour angle is:

$$\omega(\tau) = 15\tau - 180 \tag{20}$$

By substituting (19) into (20) we obtain:

$$\omega(n) = 15 n \Delta t \tag{21}$$

Taking into consideration Eqs. (18) and (21), we obtain

$$\omega(n) = \frac{360 n}{N} \tag{22}$$

or in radians

$$\omega(n) = \frac{2\pi n}{N} \tag{23}$$

In the performed calculations, the following detailed data are assumed: 1 h time intervals and a variability of solar time from 5:00 a.m. until 8:00 p.m. The data given above correspond to the variability of the hour angle from -105° to +120° and the time variable n, assuming integer values from -7 up to +8.

4. Maximum power point tracking

The PV system under investigation utilizes maximum power point tracking (MPPT). The PV MPP is predicted using type-1 fuzzy logic. MPP is pursued by varying the value of the PV output voltage.

4.1 Fuzzification

The values of membership function are assigned to the linguistic variables using five fuzzy subsets: negative big (NB), negative (N), zero (ZO), positive (P), and positive big (PB). Variables ΔV and ΔP are selected as input variables, where ΔV is the change of output voltage, $V(k)-V(k-1)$, and ΔP is the change of output power, $P(k)-P(k-1)$. The output variable is the output voltage correction, ΔU. The membership functions of the variables are shown in Fig. 3.

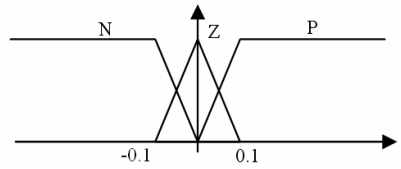

(a)

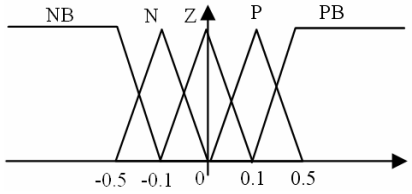

(b)

Fig. 3. Membership functions: (a) The IF-part; (b) The THEN-part

4.2 Inference method

The fuzzified inputs are fed to the inference engine, after which the rule base is applied. The output fuzzy sets are then identified using fuzzy implication method. The commonly used fuzzy implication method is MIN-MAX, which is also used in this paper. Table 2 shows the rule base adopted for the MPP tracking (MPPT); the general form of these rules is given below:

if ΔV is ... and ΔP is ..., then ΔU becomes ...

These rules are chosen according to previous knowledge regarding the system and via some trial-error processes.

Table 2. The rule base adopted for the MPPT

ΔV\ΔP	N	Z	P
N	PB	P	N
Z	P	Z	N
P	NB	N	P

4.3 Defuzzification

After fuzzy implication, the output fuzzy region is located. Because the final desired output is a non-fuzzy value, a defuzzification stage is needed. The center of gravity defuzzification method is used for defuzzification in the proposed MPPT.

5. Type-2 fuzzy logic optimizer

The structure of type-2 fuzzy logic optimizer (T2FLO) of sizing ratio (R) is shown in Fig. 4. Inputs of T2FLO are the change of hourly average power generated during hours of sunshine of 1 year, ΔP_a, and change of sizing ratio, ΔR, where $\Delta P_a = P_a(k) - P_a(k-1)$ and $\Delta R = R(k) - R(k-1)$.

Output is the correction of sizing ratio: dR.

Therefore, the sizing ratio in the k^{th} iteration is given by $R(k) = R(k-1) + dR$.

The rated PV array capacity has been fixed according to Table 1 as follows:

$$P_{pv,rated} = 35 \times 3.15 \times 7 \times 17 = 13 KW_p$$

The rated inverter input power at k^{th} iteration is calculated as follows:

$$P_{inv,rated}(k) = P_{pv,rated} \times R(k)$$

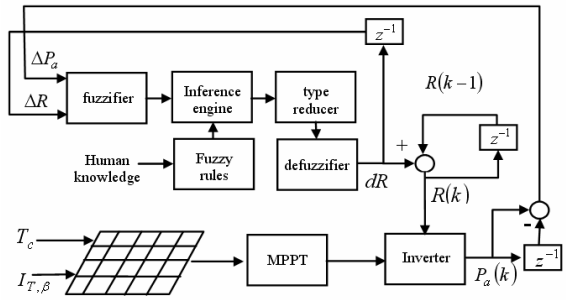

Fig. 4. The structure of type-2 fuzzy logic optimizer.

Assume that there are M rules in the type-2 fuzzy system, each of which has the following form:

Rule i: IF ΔP_a is $\tilde{G}^i_{\Delta P_a}$ and ΔR is $\tilde{G}^i_{\Delta R}$, THEN dR is $[w^i_l, w^i_r]$

where $i = 1, 2.., M$, $\tilde{G}^i_{\Delta P_a}$ and $\tilde{G}^i_{\Delta R}$ are the interval type-2 fuzzy sets of the IF part, and w^i_l and w^i_r are the singleton upper and lower values of the THEN part, respectively. The membership functions of the IF part and THEN part are shown in Fig. 5. The fuzzy labels are NB, negative small (NS), ZO, positive small (PS), and PB. The firing interval of the i^{th} rule can be obtained as follows:

$$F^i = [\underline{f}^i \quad \overline{f}^i] \tag{24}$$

where

$$\underline{f}^i = \underline{\mu}_{\tilde{G}^i_{\Delta P}}(\Delta P_a) \times \underline{\mu}_{\tilde{G}^i_{\Delta R}}(\Delta R) \tag{25}$$

$$\overline{f}^i = \overline{\mu}_{\tilde{G}^i_{\Delta P}}(\Delta P_a) \times \overline{\mu}_{\tilde{G}^i_{\Delta R}}(\Delta R) \tag{26}$$

in which $\underline{\mu}(.)$ and $\overline{\mu}(.)$ denote the grade of the lower membership function and the upper membership function, respectively.

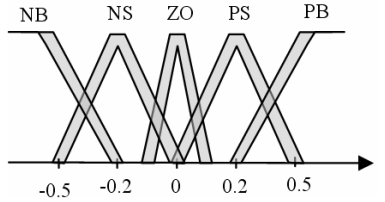

(a)

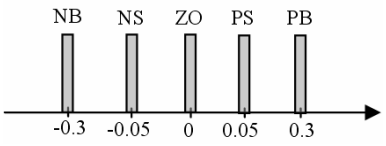

(b)

Fig. 5. Membership function: (a) The IF part; (b) The THEN part

the singleton fuzzification with a minimum t-norm used in this work is shown in Fig. 6.

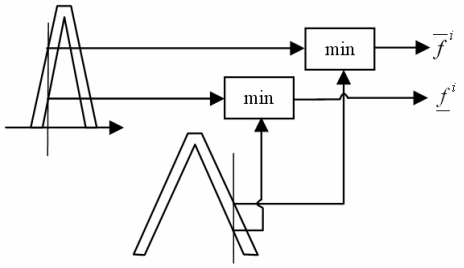

Fig. 6. Fuzzification

Many methods are used to perform type reduction. The most common is the center-of-set type reducer utilized in this paper. The output of the type reducer can be expressed as follows:

$$dR_{\cos} = [dR_l, dR_r] \tag{27}$$

where $dR_{\cos}$ is an interval type-1 set determined by the left and right points (dR_l and dR_r), which can be derived from the consequent centroid set $[w_l^i, w_r^i]$ and firing strength $f^i \in F^i = [\underline{f}^i \quad \overline{f}^i]$. The interval set $[w_l^i, w_r^i]$ ($i = 1, 2, \ldots, M$) should first be computed or set before the computation of $dR_{\cos}$. The leftmost point dR_l and the rightmost point dR_r can be expressed as [7, 8]

$$dR_l = \frac{\sum_{i=1}^{M} f_l^i w_l^i}{\sum_{i=1}^{M} f_l^i} \tag{28}$$

And

$$dR_r = \frac{\sum_{i=1}^{M} f_r^i w_r^i}{\sum_{i=l}^{M} f_r^i}. \tag{29}$$

Here, dR_l and dR_r can be computed efficiently using the Karnik-Mendel algorithm [29]: sort w_r^i (i = 1, 2, ..., M) in increasing order and call the sorted w_r^i by the same name (now $w_r^1 \le w_r^2 \le \cdots \le w_r^M$), match the weights F^i with their respective w_r^i and renumber them such that their index corresponds to the renumbered w_r^i.

Step 1: Compute dR_r in Eq. (29) by initially using $f_r^i = \left(\underline{f}^i + \overline{f}^i\right)/2$ for $i = 1, 2, \ldots, M$, where $\underline{f}^i$ and $\overline{f}^i$ are pre-computed by Eqs. (25) and (26), and let $dR_r' = dR_r$.

Step 2: Find $k\left(1 \le k \le M-1\right)$ such that $w_r^k \le dR_r' \le w_r^{k+1}$.

Step 3: Compute dR_r in Eq. (29) with $f_r^i = \underline{f}^i$ for $i \le k$, and $f_r^i = \overline{f}^i$ for $i > k$, then set $dR_r'' = dR_r$.

Step 4: If $dR_r'' \ne dR_r'$, go to Step 5; if $dR_r'' = dR_r'$, then set $dR_r = dR_r''$ and go to Step 6.

Step 5: Let $dR_r' = dR_r''$ and return to Step 2.

Step 6: End.

Hence, dR_r in Eq. (29) can be re-expressed as:

$$dR_r = \frac{\sum_{i=1}^{k} \underline{f}^i w_r^i + \sum_{i=R+1}^{M} \overline{f}^i w_r^i}{\sum_{i=1}^{k} \underline{f}^i + \sum_{i=R+1}^{M} \overline{f}^i} \tag{30}$$

The procedure to compute dR_l is similar to that for dR_r with slight modifications, as stated below. In Step 2, $k\left(1 \le k \le M-1\right)$ must be found, such that $w_l^k \le dR_l' \le w_l^{k+1}$. In step 3, let $f_l^i = \overline{f}^i$ for $i \le k$, and $f_l^i = \overline{f}^i$ for $i > k$.

Therefore, dR_l in Eq. (29) can be expressed as

$$dR_l = \frac{\sum_{i=1}^{k} \overline{f}^i w_l^i + \sum_{i=L+1}^{M} \underline{f}^i w_l^i}{\sum_{i=1}^{k} \overline{f}^i + \sum_{i=L+1}^{M} \underline{f}^i} \tag{31}$$

Then, the defuzzified crisp output from an interval type-2 fuzzy system is the average of dR_r and dR_l:

$$dR = \frac{dR_l + dR_r}{2} \tag{32}$$

The fuzzy rules are summarized in Table 3, which is constructed for the scenario wherein ΔP_a and ΔR approach zero as fast as possible and without an overshoot of the optimum value of R. Generally, the determination

of these rules comes from human knowledge and via some trial-error processes.

Table 3. Fuzzy rules.

	NB	NS	ZO	PS	PB
NB	PB	PB	NS	NS	NB
NS	PS	PB	ZO	ZO	NS
ZO	NS	ZO	ZO	PS	NS
PS	NS	NB	ZO	PS	PB
PB	NS	NS	ZO	PS	PB

6. Simulation results

Using synthetic data generated by PVSYS, sizing ratio is defined in terms of total system output and using type-2 fuzzy logic, for four locations in Algeria: Batna (35.35°N, 6.1°E), Algiers (36.43°N, 3.15°E), Adrar (27.51°N, 0.17°W), and Tamanrasset (22.47°N, 5.31°E).

Fig. 7 shows the synthetic meteorological data generated by PVSYS for Batna (East Algeria).

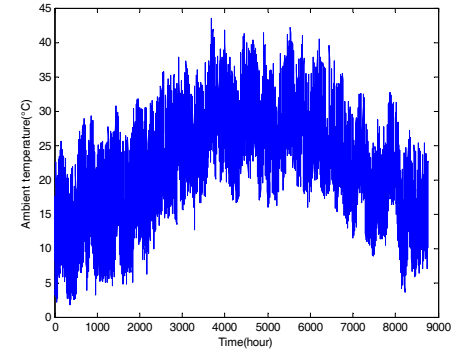

(a)

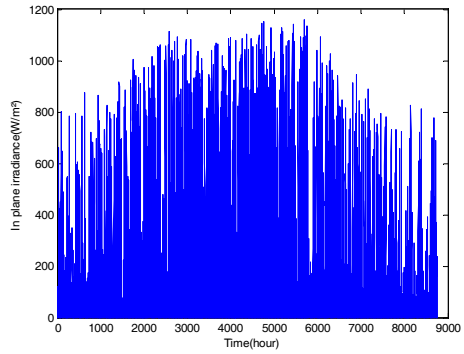

(b)

Fig. 7. Meteorological data for Batna Ambient temperature Global in-plane insolation

The results obtained using type-2 fuzzy logic to find the optimum sizing ratio between the rated inverter input power and the PV array capacity at STCs for this location are shown in Fig. 8. The optimum sizing ratio is 1.291 for tilted angle $\beta = 45°$ and 1.204 for $\beta = 60°$.

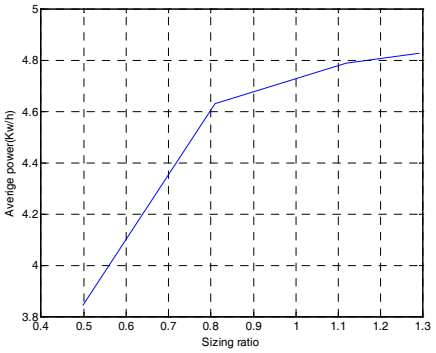

(a)

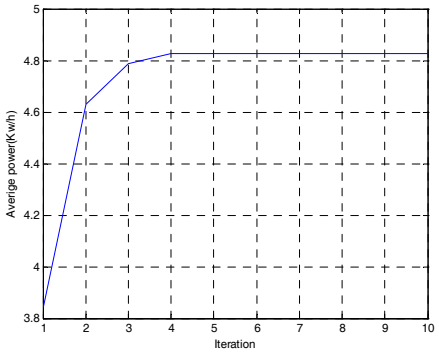

(b)

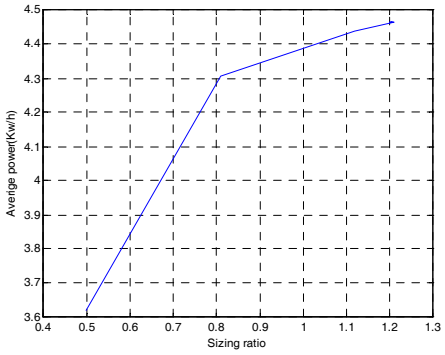

(c)

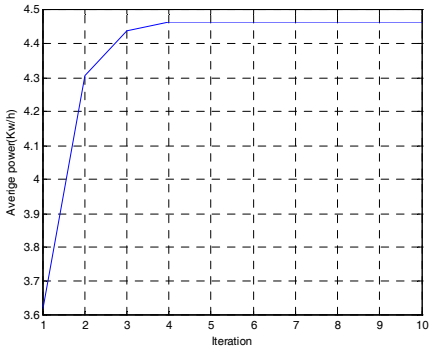

(d)

Fig. 8. Results obtained for Batna: (a) and (b) $\beta = 45°$; (c) and (d) $\beta = 60°$

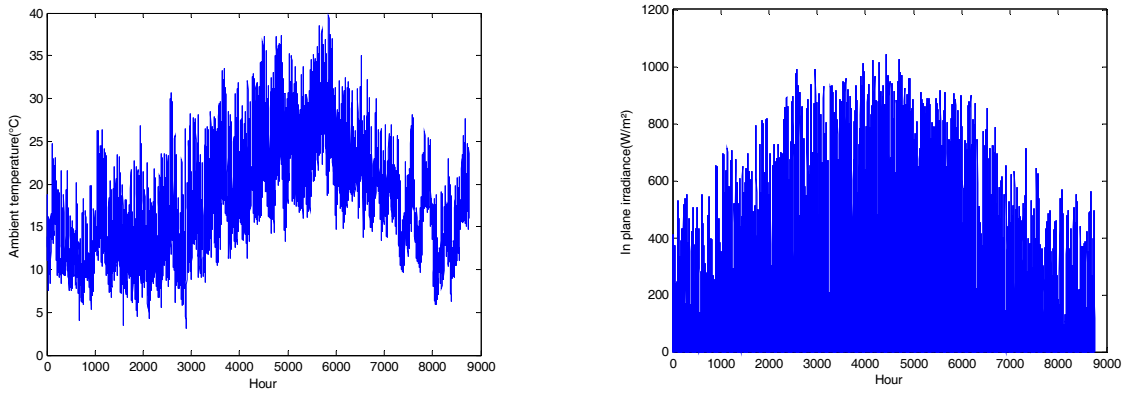

(a) (b)

Fig. 9. Meteorological data for Algiers: (a) Ambient temperature; (b) Global in-plane insolation

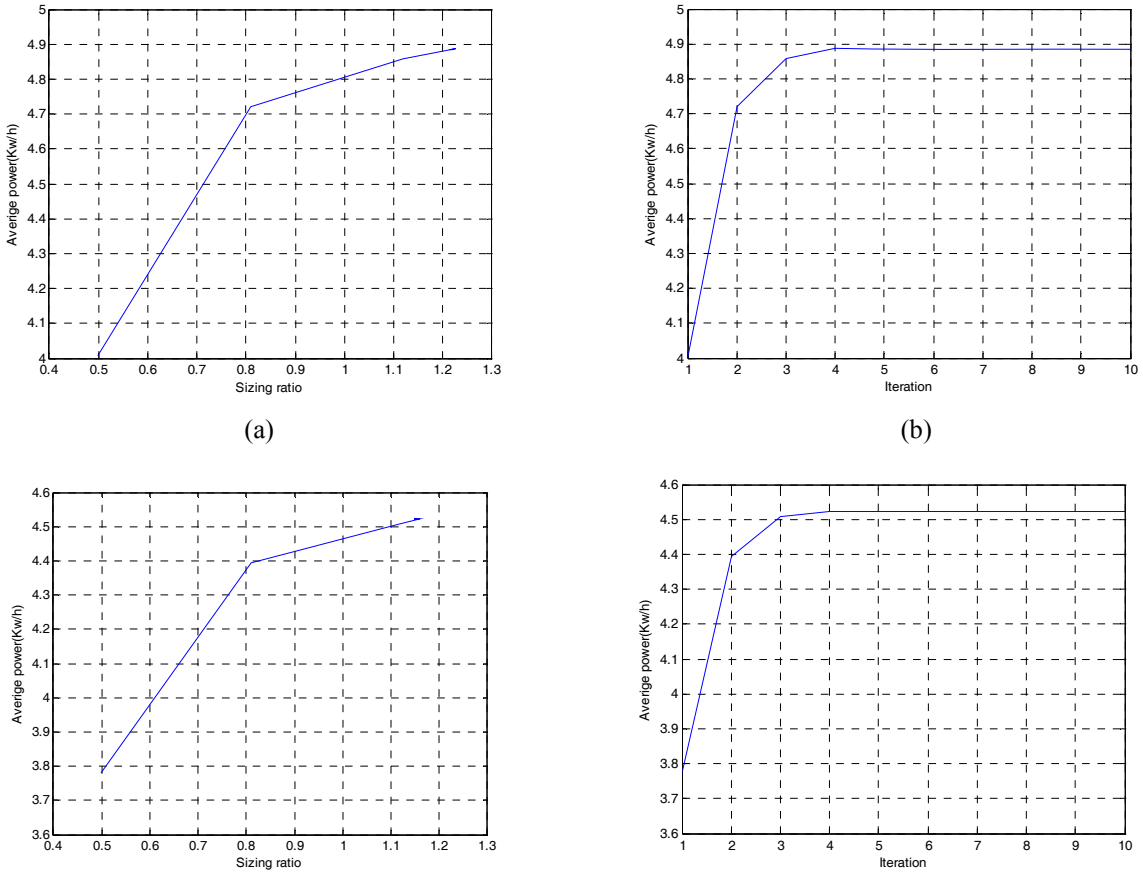

(a) (b)

(c) (d)

Fig. 10. Results obtained for Algiers: (a) and (b) $\beta = 45°$; (c) and (d) $\beta = 60°$

Fig. 9 shows the synthetic meteorological data generated by PVSYS for Algiers (North Algeria).

The results obtained for this location are shown in Fig. 10. The optimum sizing ratio is 1.220 for tilted angle $\beta = 45°$ and 1.153 for $\beta = 60°$.

Fig. 11 shows the synthetic meteorological data generated by PVSYS for Adrar (Southwest Algeria).

The results obtained for this location are shown in Fig. 12. The optimum sizing ratio is 1.321 for tilted angle $\beta = 45°$ and 1.210 for $\beta = 60°$.

Fig. 13 shows the synthetic meteorological data generated by PVSYS for Tamanrasset (Southeast Algeria).

The results obtained for this location are shown in Fig. 14. The optimum sizing ratio is 1.451 for tilted angle $\beta = 45°$ and 1.321 for $\beta = 60°$

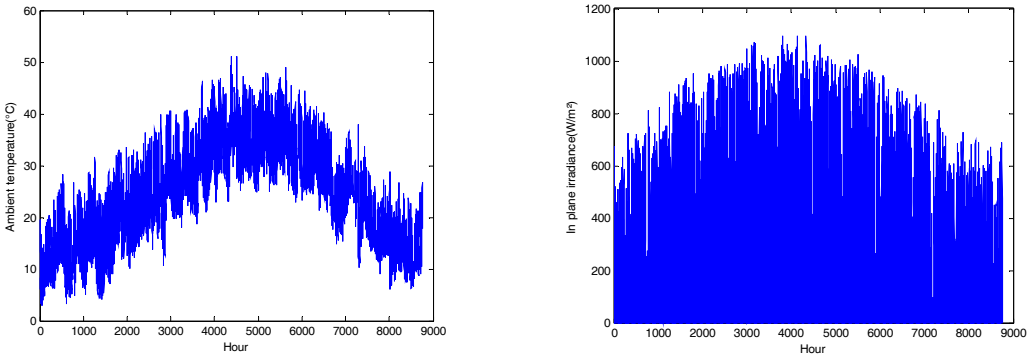

(a) (b)

Fig. 11. Meteorological data for Adrar: (a) Ambient temperature; (b) Global in-plane insolation

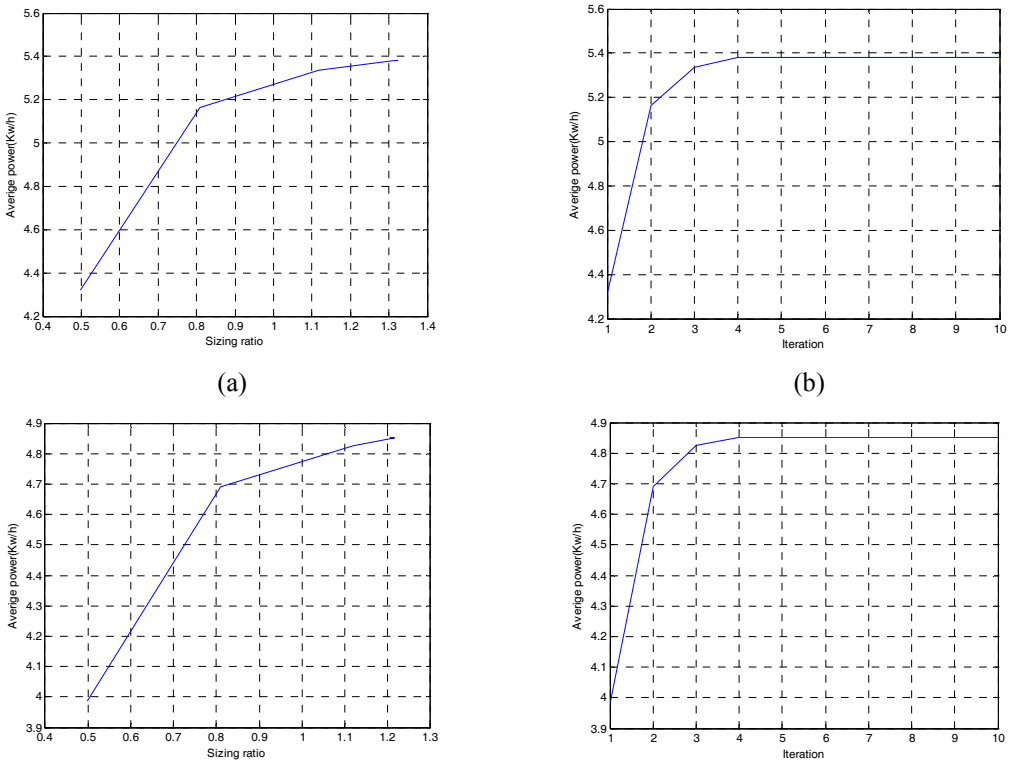

(a) (b)

(c) (d)

Fig. 12. Results obtained for Adrar: (a) and (b) $\beta = 45°$; (c) and (d) $\beta = 60°$

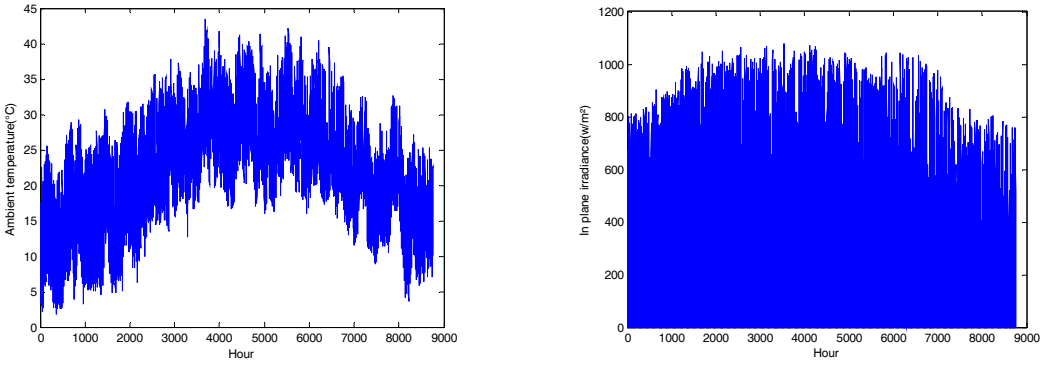

(a) (b)

Fig. 13. Meteorological data for Tamanrasset; (a) Ambient temperature; (b) Global in-plane insolation

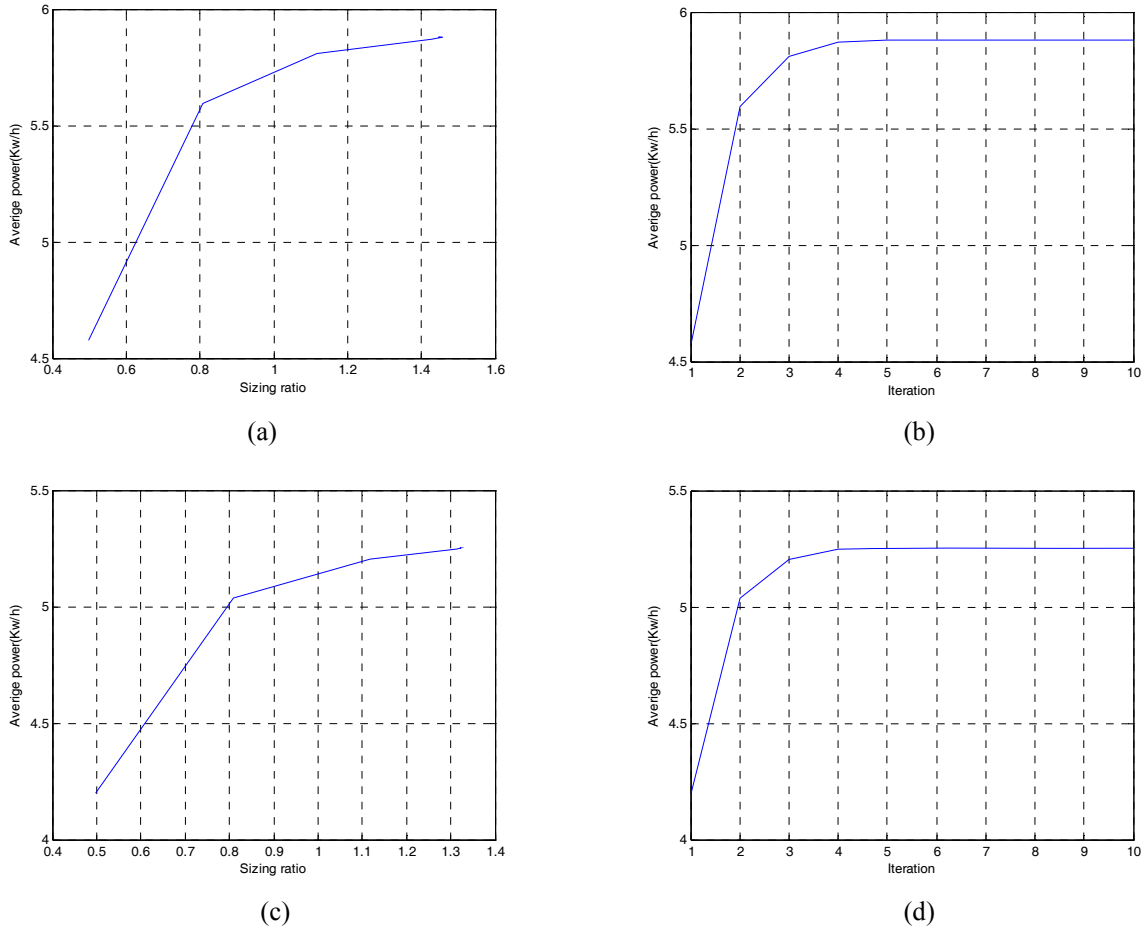

Fig. 14. Results obtained for Tamanrasset; (a) and (b) $\beta = 45°$; (c) and (d) $\beta = 60°$.

7. Conclusion

Optimum PV/inverter sizing ratios for grid-connected PV systems in selected Algerian locations were determined in terms of total system output using type-2 fuzzy logic. Because measured data in the locations chosen were unavailable, for each location, a year of synthetic hourly meteorological data generated by the PVSYST software was used in the simulation. Results show that using type-2 fuzzy logic leads to the optimum sizing ration in only four iterations. The sizing ration was defined for two tilted angles: 45° and 60°. For all locations, system provides more power for 45° than for 60° tilted angle; however, the sizing ratio is higher for 45° than for 60° tilted angle. This means that the cost of the system will be much greater. A practical technical-economical study must be conducted to define the optimum tilted angle.

References

[1] N.E. Rasmussen, H.M. Branz, "The dependence of delivered energy on power conditioner electrical characteristics for utility-interactive PV systems". In: 15th IEEE Photo-voltaic Specialists Conference, Kissimmee, Florida, USA, 1981.

[2] L. Keller, P. Aff olter, "Optimizing the panel area of a photovoltaic system in relation to the static inverter-practical results". Solar Energy 55, 1995, pp. 1-7.

[3] G. Nofuentes, G. Almonacid, "An approach to the selection of the inverter for architecturally integrated photovoltaic grid-connected systems". Renewable Energy 15, 1998, pp. 487-490.

[4] D.J. Mondol et al., "Comparison of measured and predicted long term performance of grid connected photovoltaic system". Energy Conversion And Management 48, 2007, pp. 1065-1080.

[5] D.J. Mondol et al., "Optimal sizing of array and inverter for grid-connected photovoltaic systems". Solar Energy 80, 2006, pp. 1517-1539.

[6] S. Owczarek, "Vector model for calculation of solar radiation intensity and sums incident on tilted surfaces. Identification for the three sky condition in Warsaw". Renewable Energy, Vol. 11, No. 1, 1997, pp. 77-96.

[7] N.N. Kamik, , J.M. Mendel, and Q. Liang, "Type-2 fuzzy logic system", IEEE Trans. Fuzzy Syst., 2000, 8, (5), pp. 535-550.

[8] Q. Liang, N. Kamik and J. Mendel, "Connection admission control in ATM networks using survey-based type-2 fuzzy logic system", IEEE Trans. Syst. Man Cybern. C, Appl. Rev., 30, (4), 2000, pp.329-339.
[9] G. Notton, et al., "Predicting hourly solar irradiations on inclined surfaces based on the horizontal measurements: Performances of the association of well-known mathematical models". Energy Conversion and Management 47, 2006, pp. 1816-1829.
[10] W. Coppye , W. Maranda , Y. Nir , L. De Gheselle, J. Nijs, "Detailed comparison of the inverter operation of two grid-connected PV demonstration systems in Belgium". In: 13th European Photovoltaic Solar Energy Conference, Nice, France, 1995, pp 1881-1884.
[11] B. Burger, R. Rüther, "Inverter sizing of grid-connected photovoltaic systems in the light of local solar resource distribution characteristics and temperature". Solar Energy 80, 2006, pp. 32-45.
[12] W. Marańda, G.D. Mey, A.D. Vos, "Optimization of the master–slave inverter system for grid-connected photovoltaic plants". Energy Conversion and Management 39, 1998, pp. 1239-1246.
[13] M.H. Macagnan, E. Lorenzo, "On the optimal size of inverters for grid connected PV systems". In: 11th European Photovoltaic Solar Energy Conference, Montreux, Switzer-land, 1992, pp. 1167-1170.
[14] M. Jantsch, H. Schmidt, J. Schmid, "Results of the concerted action on power conditioning and control". In: 11th Photovoltaic Solar Energy Conference, Montreux, Switzer-land , 1992, pp. 1589-1593.
[15] A. Louche, G. Notton, P. Poggi, G. Peri, "Global approach for an optimal grid connected PV system sizing". In: 12th European Photovoltaic Solar Energy Conference, Amsterdam, The Netherlands, 1994, pp. 1638-1641.
[16] D.J. Mondol et al., " Solar radiation modelling for the simulation of photovoltaic systems", Renewable Energy 33, 2008, pp 1109-1120
[17] A. Mellit et al., "Artificial intelligence techniques for sizing photovoltaic systems: A review", Renewable and Sustainable Energy Reviews, 2008.
[18] O. Perpiñan et al., "On the complexity of radiation models for PV energy production calculation", Solar Energy 82, 2008, pp. 125-131
[19] A. Mellit et al., "Methodology for predicting sequences of mean monthly clearness index and daily solar radiation data in remote areas: Application for sizing a stand-alone PV system", Renewable Energy 33, 2008, pp 1570-1590.
[20] R.J. Aguiar et al., "Simple procedure for generating sequences of daily radiation values using a library of Markov transition matrices". Solar Energy Vol 40, N°3, 1988, pp 269-279.
[21] R.J. Aguiar, M. Collares-Pareira, "TAG: a time-dependent, autoregressive, Gaussien model for generating synthetic hourly radiation". Solar Energy Vol 49, No 3, 1992, pp 167-174.
[22] M. Iqbal, "An introduction to solar radiation". Canada: Academic Press; 1983, ISBN 0-12-373752-4.
[23] PVSYST V4.37 Study of photovoltaic systems (Help manual).
[24] B.Bouzidi et al., "Assessment of a photovoltaic pumping system in the areas of the Algerian Sahara", Renew Sustain Energy Rev, 2008.
[25] TU. Townsend, "A method for estimating the long-term performance of direct-coupled photovoltaic". MS thesis, Solar Energy Laboratory, University of Wisconsin, Madison (USA), 1989.
[26] JA. Duffie, WA. Beckman, "Solar engineering of thermal processes". 2nd ed. John Wiley and sons; 1991.
[27] L.A. Zadeh: "The concept of a linguistic variable and its application to approximate reasoning", Inf. Sci., 1975, 8, pp. 199-249.
[28] Q. Liang and J.M. Mendel: "Interval type-2 fuzzy logic systems: theory and design", IEEE Trans. Fuzzy Syst., 2000, 8, (5), pp. 535-550.
[29] J. M. Mendel: "Uncertain Rule-Based Fuzzy Logic Systems: Introduction and New Directions", Upper Saddle River, NJ: Prentice-Hall, 2001.
[30] http://eosweb.larc.nasa.gov/sse/

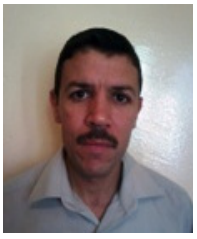

Salim MAKHLOUFI received his Magister degree in Electronic Engineering from the University of Batna, Algeria, and his Master degree in Automatics from Ecole Centrale de Nantes, France, in 2002 and 2003, respectively. At present, he is a lecturer at the University of Adrar, Algeria. His research interests include photovoltaic systems and intelligent control methods.

Rachid ABDESSEMED received his M.Sc. and Ph.D. degrees in Electrical Engineering from Kiev Polytechnic Institute, Kiev, Ukraine in 1978 and 1982, respectively. He is currently a Professor in the Department of Electrical Engineering, Batna University, Algeria. He is also Director of the Electrical Engineering Laboratory. His research interests include design and control of induction machines, as well as renewable energy.